Spatially-mapped single-cell chromatin accessibility

Casey A. Thornton[1], Ryan M. Mulqueen[1], Kristof A. Torkenczy[1], Eve G. Lowenstein[1], Andrew J. Fields[1], Frank J. Steemers[2], Kevin M. Wright[3], Andrew C. Adey[1,4,5,6,*]

1) Molecular and Medical Genetics, Oregon Health & Science University, Portland, OR.
2) Illumina Inc. San Diego, CA
3) The Vollum Institute, Oregon Health & Science University, Portland, OR.
4) CEDAR, Oregon Health & Science University, Portland, OR.
5) Knight Cancer Institute, Oregon Health & Science University, Portland, OR.
6) Knight Cardiovascular Institute, Oregon Health & Science University, Portland, OR.
* To whom correspondence should be addressed: adey@ohsu.edu

Abstract

High-throughput single-cell genomic assays resolve the heterogeneity of cell states in complex tissues, however, the spatial orientation within the network of interconnected cells is lost. As cell localization is a necessary dimension in understanding complex tissues and disease states, we present a novel method for highly-scalable spatially-resolved single-cell profiling of chromatin states. We use high density multiregional sampling to perform single-cell combinatorial indexing on Microbiopsies Assigned to Positions for the Assay for Transposase Accessible Chromatin (sciMAP-ATAC) to produce single-cell data of equivalent quality to non-spatial single-cell ATAC-seq. We apply sciMAP-ATAC in the adult mouse cortex to discriminate cortical layering of glutamatergic neurons and establish the spatial ordering of single cells within intact tissue. We then leverage this spatially-oriented cell dataset by combining it with non-spatially resolved whole brain sci-ATAC-seq data and assess layer-specific marker gene chromatin accessibility and transcription factor motif enrichment. Using sciMAP-ATAC seq, we identify sets of regulatory elements that spatially vary in the cortex, which includes canonical layer-specific markers and previously unannotated putative regulatory elements.

Introduction

Complex networks of heterogeneous cell types coordinate to generate the emergent properties of tissues. In addition to the complexity of cellular networks, many organs have spatially localized functionality. Moreover, in disease states, many organs experience spatially progressive etiologies. With the advent of next generation sequencing, many methods have emerged to characterize the molecular profiles of cells in unperturbed and perturbed systems by sequencing transcriptomic, genomic, and epigenomic cellular content. Single-cell technologies have further advanced these efforts by enabling the isolation of signal from individual cells within a sample, thus resolving the heterogeneity of complex tissues. Applications of single-cell technologies have identified novel cell types with characteristic -omic signatures, and have revealed pathogenesis and clonal expansion in cancers such as acute myeloid leukemia[1,2] and pancreatic ductal adenocarcinoma[3,4]. While these advances have revolutionized cellular taxonomy and quantification of tissue heterogeneity, the spatial orientation of the single cells is not recorded due to whole-sample dissociation.

To address this challenge, several strategies have emerged to assay transcription either directly *in situ* or in a regional manner. The former techniques utilize fluorescence *in situ* hybridization (FISH)[5–7] or *in situ* RNA-sequencing[8,9]. While powerful, FISH methods are difficult to perform, require the use of a defined probe set, and are generally limited to the study of RNA transcription. In contrast, technologies that utilize array-based mRNA barcoding do not require a defined set of genes and operate similarly to single-cell RNA-seq methods[10,11], thus allowing for whole-genome transcriptome profiling. Initial iterations of these platforms capture regional transcription over multiple cells; however, higher resolution variants may facilitate single-cell resolution. Unfortunately, these platforms rely on the relatively easy access to mRNA molecules that can be released from the cytoplasm and hybridized to barcoding probes, making the expansion into nuclear epigenetic properties challenging. With the wealth of epigenetic information that resides in the nucleus, and the value it can have on characterizing a complex biological system[12–14], we sought to address this challenge by harnessing the inherent throughput characteristics of single-cell combinatorial indexing assays[15,16].

Here, we present single-cell combinatorial indexing from Microbiopsies with Assigned Positions for the Assay for Transposase Accessible Chromatin (sciMAP-ATAC). sciMAP-ATAC preserves cellular localization within intact tissues and generates thousands of spatially-resolved high quality single-cell ATAC-seq libraries. As with other 'sci-' technologies, sciMAP-ATAC does not require specialized equipment and scales nonlinearly, enabling high throughput potential. Building upon multiregional sampling strategies[17,18], we reasoned that the sample multiplexing capabilities of combinatorial indexing could be utilized to perform high throughput multiregional sampling at resolutions approaching those of array-based spatial transcriptional profiling, all while retaining true single-cell profiles. Unlike multiregional sampling, where several regions are isolated, we perform high-density microbiopsy sampling, ranging from 100-500 µm in diameter, on cryosectioned tissue slices, between 100-300 µm in thickness, to produce up to hundreds of spatially-mapped samples, each of which produces a set of single-

cell chromatin accessibility profiles (Figure 1a). We demonstrate the utility of sciMAP-ATAC by profiling the murine brain where distinct cell type compositions and chromatin profiles are observed based on the spatial orientation of the punches.
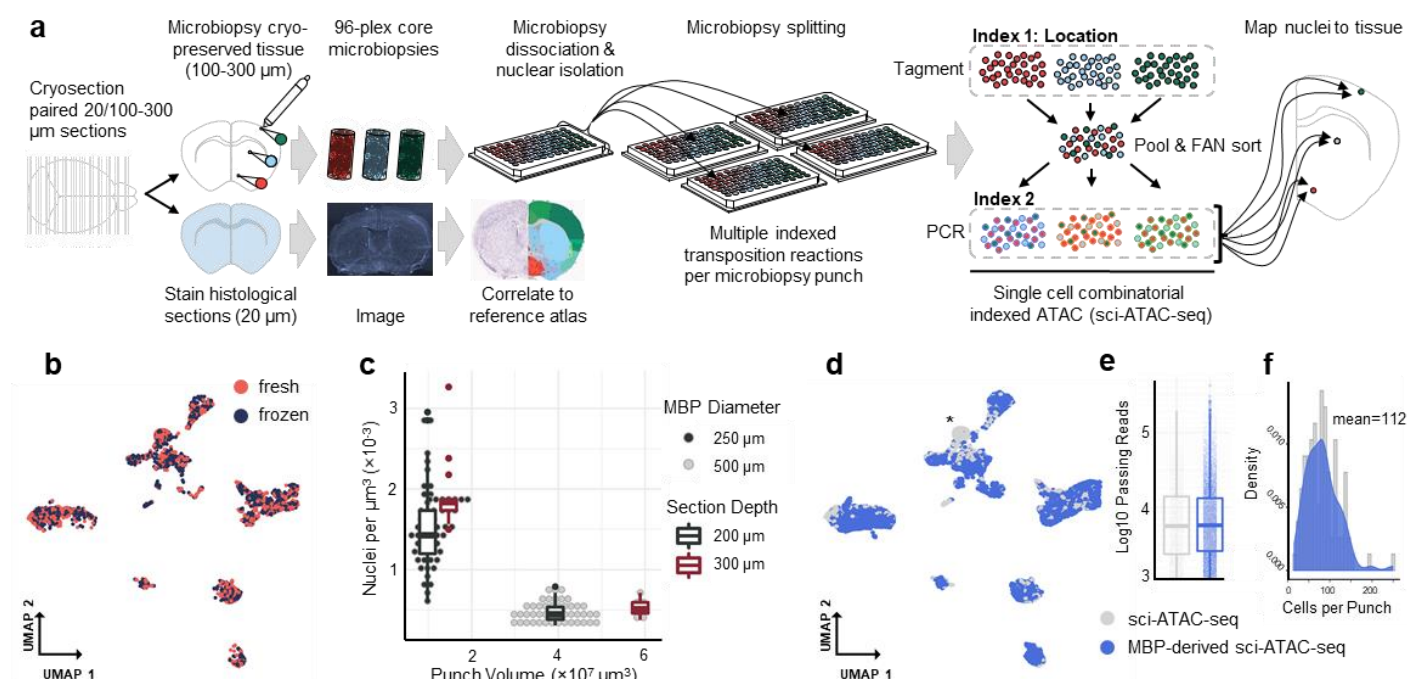
Figure 1 | sciMAP-ATAC schematic and performance. a. sciMAP-ATAC workflow. Cryosectioning of alternating 20 μm (imaging) and 100-300 μm (MBP) slices are obtained. Thin (20 μm) slices are stained and imaged for use in spatial registration. Thick (100-300 μm) slices are carried through high-density microbiopsy punching (100-300 μm diameter) in the cryostat chamber. MBPs are placed directly into wells of a microwell plate for nuclei isolation and washing prior to splitting into multiple wells for indexed transposition and the sci-ATAC-seq workflow. **b.** sci-ATAC-seq performed on mouse whole-brain samples from fresh or flash frozen using cryosectioning methods produce comparable profiles. **c.** Nuclear dissociation from mouse brain microbiopsies yield on average 14,938 nuclei (1.5×10^{-3} nuclei/μm³) for 250 μm × 200 μm cylindrical microbiopsies. Higher nuclei extraction efficiencies are observed for smaller diameter punches. **d.** MBP-derived sci-ATAC-seq libraries group closely with standard sci-ATAC-seq libraries. Asterisk indicates a population of 734 cells, derived from spinal cord which was not sampled during microbiopsy punching. **e.** Passing reads per cell from MBP-derived sci-ATAC-seq (mean of 12,052) is comparable to standard sci-ATAC-seq (mean of 11,978) methods. **f.** Distribution of passing cells per MBP (mean of 112) across 384 punches.

Results

Single-cell combinatorial indexed ATAC-seq from microbiopsy punches

Single-cell ATAC-seq requires the isolation and processing of nuclei such that the nuclear scaffold remains intact in order to facilitate library preparation via transposition *in situ,* and that the chromatin structure is maintained in order to produce chromatin accessibility signal. We and others have explored methods for tissue preservation that are compatible with single-cell ATAC-seq[15,19], however, we needed to confirm that these strategies are compatible with freezing techniques used for cryosectioning. We tested our workflow on mouse whole-brain samples by processing one hemisphere using flash-freezing methods designed for OCT-embedding and

cryosectioning and the other processed directly as fresh tissue. Both samples were processed according to our sci-ATAC-seq workflow[19] and pooled post-transposition for sorting, PCR amplification, and sequencing. Flash-frozen nuclei co-cluster indiscriminately with non-spatially resolved sciATAC-seq nuclei, indicating that flash-freezing methods compatible with cryosectioning does not disrupt chromatin structure (Figure 1b). These preparations showed nearly identical quality metrics between fresh and flash-frozen samples and serve as a baseline for subsequent spatial experiments (Extended Data Figure 1).

We then explored techniques for cryosectioning flash-frozen OCT-embedded tissue at thicknesses compatible with microbiopsy punching (MBP). Typically, cryosectioning is used to produce slices for imaging applications and thicker slicing results in tissue fracture. Drawing on past literature[20], we carried out a series of experiments testing several sectioning thicknesses and MBP diameters as well as nuclei isolation and washing conditions on flash-frozen, OCT-embedded mouse brain microbiopsy punches. We found that increasing cryo-chamber and chuck temperatures to -11°C increases flexibility of the fragile fresh-frozen tissue, while maintaining adherence of embedded tissue to the chuck, thus allowing for uninterrupted sectioning of alternating 100-300 µm sections for MBP, and paired 20 µm sections for histology (Figure 1a). While this method of cryosectioning thick sections reduces the quality of the immediately adjacent thin histological section due to shearing forces, we find that these sections are sufficient for determining the coordinates of the tissue within the mouse brain. This approach facilitates slide processing, fixation, and staining according to the tissue used and any given experimental design. Additionally, cryopreservation of 100-300 µm/20 µm slide decks at -80°C allows for long-term sample storage and the ability to stain for markers of interest post spatially resolved single-cell epigenomic profiling using sciMAP-ATAC.

Microbiopsy punching of 100 µm-300 µm sections performed within a cooled chamber (-20°C) allows for isolation of microscopic pellets of nuclei which readily dissociate in nuclear isolation buffer post mechanical dissociation by trituration. We observed minimal loss after pelleting and washing nuclei, an important step for the removal of mitochondria, which can deplete the available pool of transposase due to the high transposition efficiency into mitochondrial DNA[21]. Overall, nuclei isolation was more efficient, as measured by nuclei per cubic micron, for volumetrically smaller punches (Figure 1c). This finding implies that smaller MBP dissociate more readily due to higher tissue surface area per cell, thus higher resolution punches volumetrically yield more nuclei.

Next, we utilized our established workflow for sci-ATAC-seq, with each indexed transposition reaction performed on an individual microbiopsy-derived nuclei preparation, for a total of 384 transposition reactions. Reactions were pooled and indexed nuclei distributed via Fluorescence Assisted Nuclei Sorting (FANS) to wells of a new 96-well plate for indexed real-time PCR followed by pooling and sequencing. The resulting library performed comparable to a standard sci-ATAC-seq preparation with 8,012 total cells passing filters and a mean of 12,052 passing reads per cell (unique, mapped to autosomes or X chromosome at q10 or higher) at the depth sequenced and potential to sequence up to 23,830 mean passing reads per cell (Methods, Extended Data Figure 1). This is comparable

to the mean passing reads per cell from the whole brain sci-ATAC-seq library at 11,987 (projected mean passing reads of 24,672 and 32,029 for fresh and frozen preparations, respectively; Figure 1e, Extended Data Figure 1). We observed a fairly uniform distribution of passing cells derived from each of the 384 individual MBPs (Figure 1f), with a mean of 112, which could be increased if additional PCR plates were sorted, as the pool of indexed nuclei were not depleted during FANS.

sciMAP-ATAC in the adult mouse somatosensory cortex

In order to establish the ability of sciMAP-ATAC to characterize single cells within a spatially organized tissue, we applied the technique to resolve murine cortical lamination within the somatosensory cortex. We harvested intact whole-brain tissue from three wild-type C57/Bl6J adult male mice, flash-froze the embedded tissue, and prepared whole-brain slide decks of 200 μm microbiopsy slides paired with three 20 μm histological slides. In order to orient cryosections to location within the intact mouse brain, and to establish the quality of histological section prepared according to the sciMAP-ATAC protocol, we stained with DAPI and for Satb2 (Figure 2a). The DAPI imaging was then matched to the adult mouse Allen Brain Reference Atlas[22], which enabled us to determine the somatosensory cortex location within adjacent sections for MBP acquisition. The Satb2 imaging demonstrated the quality of histological sections, across diverse fixation protocols (4% PFA post-fixation for 10 minutes, 70% ethanol post-fixation for 30 seconds) and were able to generate high signal to noise ratio canonical Satb2 IHC staining spanning layers 2-5, ref. [23] (Figure 2b). Microbiopsy punches were then taken from outer (L2-4) and inner (L4-6) somatosensory cortical layers and from throughout the striatal white matter, in order to provide an outgroup and to bolster neuroglia signal which are in higher abundance in the white matter. In total, 96, 250 μm diameter MBPs were obtained, split evenly between the three categories over seven sequential coronal sections spanning the somatosensory cortex. After nuclei isolation, each well of the plate containing a single MBP was split across four total 96-well plates for subsequent indexed transposition, providing four technical replicates for each punch. Post transposition, nuclei were pooled and distributed to two 96-well PCR plates for the second tier of indexing and then sequenced using previously described protocols[19].

We processed the raw sequence data as previously described[19], which resulted in 7,779 cells passing quality filters. Our mean passing reads per cell was 17,388, with a projected total passing mean reads per cell of 37,079 (Methods, Extended Data Figure 1). The distribution of single-cell profiles obtained per-punch was also uniform and fit a normal distribution with a median of 81 cells obtained per MBP, with little bias with respect to transposase index, MBP target region, or slice (Extended Data Figure 2). Subsequent peak calling, topic modeling, and dimensionality reduction (Methods) revealed cell groupings that were either mixed between the three categories, or highly-enriched for MBPs derived from the cortex which was further divided by outer versus inner MBP location (Figure 2c). Using spatial information alone, we were able to designate the cortical-exclusive group of cells as excitatory neurons without the use of the underlying epigenetic information simply due to the expected absence of this population in white matter regions.
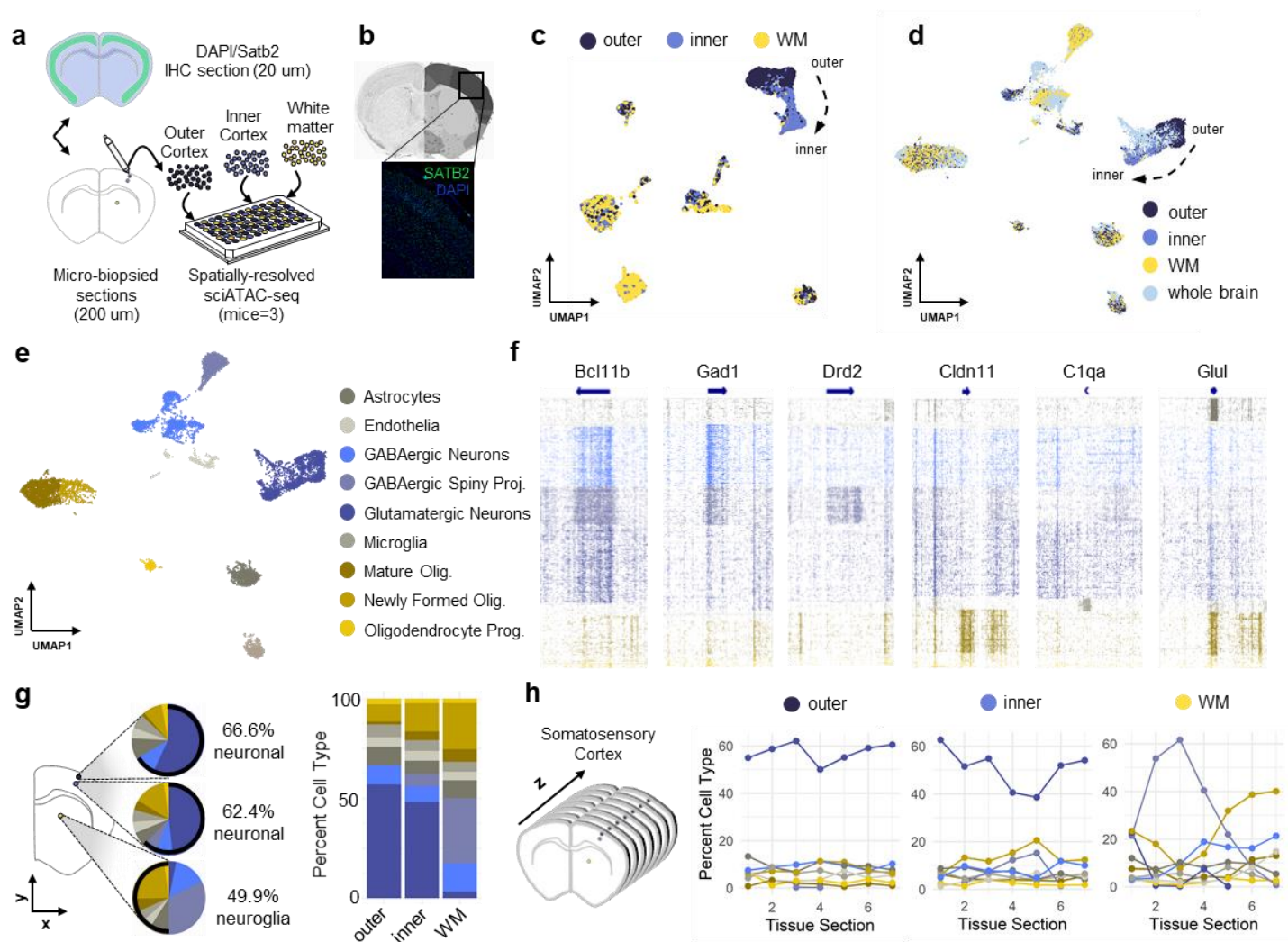
Figure 2 | sciMAP-ATAC recapitulates known features of the mouse cortex. a. Experiment schematic of sciMAP-ATAC in the mouse somatosensory cortex. Alternating 200 μm (MBP) and 20 μm (imaging) sections were produced. Seven MBP slices were used to produce equal proportions of outer, inner, and white matter (WM) 250 μm diameter MBPs that were dissociated, split to four replicate indexed transposition plates in the sciMAP-ATAC workflow. **b.** DAPI and Satb2 staining of somatosensory cortex from sciMAP-ATAC histological section. **c.** Projection by UMAP of 7,779 cells colored by punch location category. **d.** Projection of union set of spatially resolved (outer, inner, WM) cells and cells derived from whole mouse brain sci-ATAC-seq. **e.** Cell type classification of neuroglia and neurons across whole mouse brain. **f.** Chromatin accessibility signal at select cell type marker genes (full set can be found in Extended Data File 1). Each row is the signal for a single cell across the genomic region, colored by cell type classification. **g.** Cell type proportion by MBP location in xy coronal plane. **h.** Cell type proportion by sequential sections spanning somatosensory cortex (2.1mm) along rostral/caudal z-axis.

To further compare sciMAP-ATAC to non-spatial single-cell methods, we constructed a union dataset (n=19,895) which contains cells from our whole brain sci-ATAC-seq preparation on fresh and frozen tissue (n=4,104), our initial MBP-derived sci-ATAC-seq preparation from 384 whole brain derived punches (n=8,012), and our somatosensory cortex sciMAP-ATAC experiment (n=7,779). Cells from all preparations were combined and subjected to peak calling, topic modelling, and dimensionality reduction, which revealed minimal preparation bias (Figure 2d, Extended Data Figure 2). Nearly all groupings of cells were distributed across the different

experiments, with a few exceptions. One group of cells were observed exclusively in the whole brain dataset, which, upon inspection, were determined to be spinal cord derived interneurons due to enriched Hox gene chromatin accessibility (Extended Data Figure 3) and not present in regions that were isolated via spatial experiments. Additionally, a group of cells produced the same cortex-specific spatial registration when assessing the mapping of the somatosensory cortex dataset. This group had the same bias with respect to outer and inner cortical punch positioning, and contained cells from the union dataset derived from all preparations, suggesting that the spatial coordinates can be transferred to non-spatial sci-ATAC-seq preparations.

Spatially-registered cell type composition

We performed graph-based clustering to produce eleven clusters over eight broad cell type groups corresponding to glutamatergic neurons, GABAergic neurons, GABAergic medium spiny neurons (MSNs; also referred to as spiny projection neurons), oligodendrocyte precursor cells (OPCs), newly formed oligodendrocytes, mature oligodendrocytes, astrocytes, microglia, and endothelial cells based on the chromatin accessibility signature of regulatory elements proximal to marker genes (Methods, Figure 2e, Extended Data File 1). We then examined the spatial categories of microbiopsy punches which included neuronal cells mapping to outer and inner cortex microbiopsy punches correspond to excitatory neurons which are separated by punch location, and inhibitory (inter) neurons which co-cluster by cortical punch location (outer and inner). Additionally, cortical interneurons cluster separately but adjacent to white matter interneurons. This recapitulates known neuronal cell state biology, with pyramidal neurons that express cortical layer/region specific markers that define the spatially defined cortical layers. In contrast, interneurons exist sparsely and in a non-layer-specific manner in the cortex and also in the white matter. Within the somatosensory cortical microbiopsy punch derived cells (outer, inner), we observed 66.6% and 62.4% of cells corresponding to neurons, respectively. This equates to glia:neuron ratios (GNRs) of 0.49 and 0.62, respectively, and an average ratio of 0.555 across the cerebral cortex. This matches the expected mouse cerebral cortex GNR of 0.554, ref. [24] with a percent error of 0.18% (Figure 2f). In addition to xy location mapping within coronal sections by outer, inner, and white matter MBP orientation, nuclei were mapped along the rostral/caudal, or z, axis across sequential 200 μm sections (Figure 2g). We find consistently high excitatory neuron content in the outer and inner layers of the somatosensory cortex along with low-level neuroglia content, as expected. In white matter derived nuclei, we see varying levels of neuroglia content with a high percentage of GABAergic medium spiny neurons, known to populate the striatum, and persistent low-level excitatory neuron content in the white matter. These data suggest that sciMAP-ATAC captures high quality single-cell libraries which correspond to canonical cell types in proportions which correspond to the literature, across the x, y (coronal plane), and z (rostral/caudal) axes.
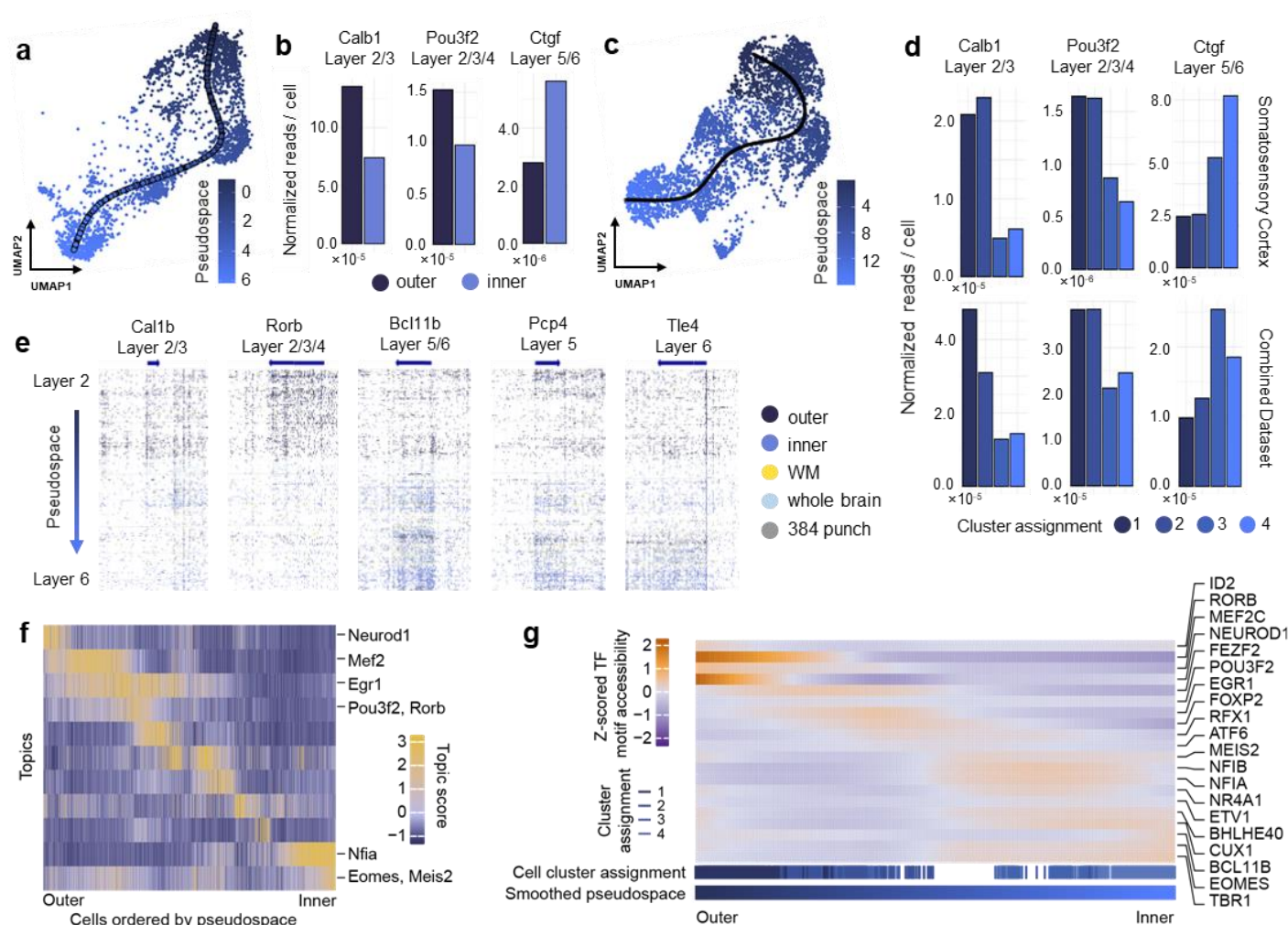
Figure 3 | Pseudospatial ordering glutamatergic neurons in the somatosensory cortex. a. Ordering of glutamatergic neurons along pseudospace according to chromatin accessibility for glutamatergic neurons derived from the somatosensory cortex sciMAP-ATAC preparation. Line represents cells projected onto linear pseudospatial principal curve (n=2,458). **b.** Mean normalized read count from somatosensory cortex sciMAP-ATAC excitatory neurons for layer specific marker genes Calb1, Pou3f2, and Ctgf. **c.** Pseudospatial ordering as in **a**, but for the union dataset (n=4,282). **d.** Layer-specific marker gene accessibility measured by normalized reads per cell for four pseudospace ordered excitatory neuron sub-clusters. Marker gene accessibility in sciMAP-ATAC somatosensory cortex excitatory neurons only (top). Marker gene accessibility for union dataset excitatory neurons (bottom). **e.** Chromatin accessibility signal at select cortex layer-specific marker genes (full set can be found in Extended Data File 2). Each row is the signal for a single cell across the genomic region, colored by MBP annotation and experiment origin. **f.** Topic weight by excitatory neurons from union dataset ordered along pseudospace. Select Homer identified significantly enriched TF motifs are highlighted for key outer and inner weighted topics (p-value<1e-8, right). **g.** TF motif enrichment (rows) per excitatory neuron (columns) ordered by pseudospace.

Pseudospatial ordering of glutamatergic neurons captures cell layer markers

We next performed pseudospatial ordering of cells by chromatin accessibility in order to orient the excitatory neuron populations from outer to inner cortex microbiopsy punches and report key epigenetic regulatory elements which uniquely vary along the axis of space. In addition to a pseudospatial analysis of the somatosensory cortex sciMAP-ATAC preparation (Figure 3a), we utilized the combined dataset of all preparations for which a clear progression from outer to inner cortical layer derived punches was observed in

the positional labels of the somatosensory cortex dataset. We reasoned that using this combined dataset is a powerful demonstration of the ability to project spatial information from sciMAP-ATAC cells to those from other preparations, much like strategies to integrate standard and multi-modal scRNA-seq datasets[25]. Cell ordering was carried out by projecting a principal curve through the two-dimensional cell embedding for both the somatosensory cortex only and combined datasets (Figure 3a,c). We next examined the chromatin accessibility patterns of layer-specific marker genes along between outer and inner MBP and at higher resolution along the pseudospatial progression (Figure 3b). Canonical upper-layer neuron marker genes Calb1 (L2/3) and Pou3f2 (L2/3/4), for example, were revealed to have higher chromatin accessibility in outer MBP as compared to inner MBP as measured by normalized read count per cell. Additionally, lower-layer markers Fezf2 (L5) and Ctgf (L5/6), for example, were found to have increased accessibility in excitatory neurons derived from inner MBP. In order to assess chromatin states of excitatory neuron cells at higher resolution, graph-based clustering was performed on the union set of excitatory neurons and four distinct sub-clusters were identified, which recapitulates previously described excitatory neuron single cell analyses[26]. Ordering of sub-clusters by mean pseudospace value reveals that layer-specific marker gene chromatin accessibility, as measure by normalized reads per cell within each sub-cluster, corresponds to expected layer enrichment across the fourteen canonical marker genes assessed (Figure 3d, Extended Data Figure 4). Additionally, ordering of each excitatory neuron cell from the union dataset by pseudospace value reveals canonical marker genes layer-specific accessibility (Figure 3e, Extended Data File 2).

In addition to examining chromatin accessibility signal, we examined topic weights through pseudospace (Figure 3f). We observed 11 topics that demonstrated clear signal progression with key motif enrichment corresponding to known factors that progress through lamination. Analysis of transcription factor (TF) binding motif enrichment revealed that outer layer weighted topics are enriched for canonical upper-layer neuron TF motifs such as Neurod1 and Mef2a while inner layer weighted topics were enriched for lower-layer TF motifs such as Nfia, Meis, and Eomes (Tbr1). To assess the role of these TFs in excitatory neurons along pseudospace, we assayed enrichment of these TF binding motifs within each cell (Figure 3g). We find clear waves of TF motif enrichment along cells ordered by pseudospace from the union dataset, thus enforcing the paradigm that we are able to resolve spatial epigenomic patterning from sciMAP-ATAC single cells and from cells which are not spatially resolved but co-cluster.

Discussion

sciMAP-ATAC provides a low-cost, highly-scalable, hypothesis-independent approach to acquiring spatially resolved epigenomic single-cell data with the use of immediately available commercial tools. Additionally, sciMAP-ATAC is translatable to any tissue, culture, or model system which can be cryosectioned. While many methods rely on signal-to-noise optical detection of densely packed molecules and computationally intensive spatial reconstruction, sciMAP-ATAC encodes nuclear localization directly into each library molecule, allowing

for rapid subsetting of cells by localization and mapping of cells across vector space in 3D. We demonstrate the use of sciMAP-ATAC to profile the murine somatosensory cortex, recapitulating known marker gene progression through cortical layering and cell type composition based on the category and positioning of spatially-registered microbiopsy punches. Application of sciMAP-ATAC to other highly structured systems or tissues with a gradient of disease phenotype will be particularly valuable areas for this technology. Furthermore, we applied the sciMAP strategy to assess chromatin accessibility; however, it can, in theory, be applied to any single-cell combinatorial indexing technique to enable spatially-registered single-cell genome, transcriptome, chromatin folding, or methylation assays.

References

1. Potter, N. *et al.* Single cell analysis of clonal architecture in acute myeloid leukaemia. *Leukemia* **33**, 1113–1123 (2019).

2. Xu, L. *et al.* Clonal Evolution and Changes in Two AML Patients Detected with A Novel Single-Cell DNA Sequencing Platform. *Sci. Rep.* **9**, 11119 (2019).

3. Peng, J. *et al.* Single-cell RNA-seq highlights intra-tumoral heterogeneity and malignant progression in pancreatic ductal adenocarcinoma. *Cell Res.* **29**, 725–738 (2019).

4. Ligorio, M. *et al.* Stromal Microenvironment Shapes the Intratumoral Architecture of Pancreatic Cancer. *Cell* **178**, 160-175.e27 (2019).

5. Lubeck, E., Coskun, A. F., Zhiyentayev, T., Ahmad, M. & Cai, L. Single-cell in situ RNA profiling by sequential hybridization. *Nat. Methods* **11**, 360 (2014).

6. Chen, K. H., Boettiger, A. N., Moffitt, J. R., Wang, S. & Zhuang, X. Spatially resolved, highly multiplexed RNA profiling in single cells. *Science (80-.).* **348**, aaa6090 (2015).

7. Eng, C.-H. L. *et al.* Transcriptome-scale super-resolved imaging in tissues by RNA seqFISH+. *Nature* **568**, 235–239 (2019).

8. Rodriques, S. G. *et al.* Slide-seq: A scalable technology for measuring genome-wide expression at high spatial resolution. *Science (80-.).* **363**, 1463 LP – 1467 (2019).

9. Vickovic, S. *et al.* High-definition spatial transcriptomics for in situ tissue profiling. *Nat. Methods* **16**, 987–990 (2019).

10. Islam, S. *et al.* Quantitative single-cell RNA-seq with unique molecular identifiers. *Nat. Methods* **11**, 163 (2013).

11. Hwang, B., Lee, J. H. & Bang, D. Single-cell RNA sequencing technologies and bioinformatics pipelines. *Exp. Mol. Med.* **50**, 96 (2018).

12. Topper, M. J., Vaz, M., Marrone, K. A., Brahmer, J. R. & Baylin, S. B. The emerging role of epigenetic therapeutics in immuno-oncology. *Nat. Rev. Clin. Oncol.* (2019). doi:10.1038/s41571-019-0266-5

13. Kato, M. & Natarajan, R. Epigenetics and epigenomics in diabetic kidney disease and metabolic memory. *Nat. Rev. Nephrol.* **15**, 327–345 (2019).

14. Hwang, J.-Y., Aromolaran, K. A. & Zukin, R. S. The emerging field of epigenetics in neurodegeneration and neuroprotection. *Nat. Rev. Neurosci.* **18**, 347 (2017).

15. Cusanovich, D. A. *et al.* Multiplex single-cell profiling of chromatin accessibility by combinatorial cellular indexing. *Science (80-.).* **348**, 910 LP – 914 (2015).

16. Vitak, S. A. *et al.* Sequencing thousands of single-cell genomes with combinatorial indexing. *Nat. Methods* **14**, 302 (2017).

17. Gerlinger, M. *et al.* Genomic architecture and evolution of clear cell renal cell carcinomas defined by multiregion sequencing. *Nat. Genet.* **46**, 225 (2014).

18. Erramuzpe, A., Cortés, J. M. & López, J. I. Multisite tumor sampling enhances the detection of intratumor heterogeneity at all different temporal stages of tumor evolution. *Virchows Arch.* **472**, 187–194 (2018).

19. Sinnamon, J. R. *et al.* The accessible chromatin landscape of the murine hippocampus at single-cell resolution. *Genome Res.* **29**, 857–869 (2019).

20. Palkovits, M. Isolated removal of hypothalamic or other brain nuclei of the rat. *Brain Res.* **59**, 449–450 (1973).

21. Corces, M. R. *et al.* An improved ATAC-seq protocol reduces background and enables interrogation of frozen tissues. *Nat. Methods* **14**, 959–962 (2017).

22. Lein, E. S. *et al.* Genome-wide atlas of gene expression in the adult mouse brain. *Nature* **445**, 168–176 (2007).

23. Alcamo, E. A. *et al.* Satb2 Regulates Callosal Projection Neuron Identity in the Developing Cerebral Cortex. *Neuron* **57**, 364–377 (2008).

24. Ventura-Antunes, L., Mota, B. & Herculano-Houzel, S. Different scaling of white matter volume, cortical connectivity, and gyrification across rodent and primate brains. *Front. Neuroanat.* **7**, 3 (2013).

25. Stuart, T. *et al.* Comprehensive Integration of Single-Cell Data. *Cell* **177**, 1888-1902.e21 (2019).

26. Gray, L. T. *et al.* Layer-specific chromatin accessibility landscapes reveal regulatory networks in adult mouse visual cortex. *Elife* **6**, e21883 (2017).

27. Picelli, S. *et al.* Tn5 transposase and tagmentation procedures for massively scaled sequencing projects. *Genome Res.* **24**, 2033–2040 (2014).

28. Bravo González-Blas, C. *et al.* cisTopic: cis-regulatory topic modeling on single-cell ATAC-seq data. *Nat. Methods* **16**, 397–400 (2019).

29. Schep, A. N., Wu, B., Buenrostro, J. D. & Greenleaf, W. J. chromVAR: inferring transcription-factor-associated accessibility from single-cell epigenomic data. *Nat. Methods* **14**, 975 (2017).

30. Muralidhar, S., Wang, Y. & Markram, H. Synaptic and cellular organization of layer 1 of the developing rat somatosensory cortex . *Frontiers in Neuroanatomy* **7**, 52 (2014).

Author Contributions

A.C.A. conceived of the idea and oversaw the work. C.A.T. performed all experiments described with assistance from A.J.F. F.J.S. and K.M.W. contributed to experimental design and data interpretation. C.A.T. performed data processing and analysis with assistance from K.A.T., R.M.M. and E.G.L. C.A.T. and A.C.A. wrote the manuscript.

Competing interests

F.J.S. is an employee of Illumina Inc.

Data and Materials Availability

The sciMAP-ATAC protocol will be made publicly available at protocols.io. The majority of analysis was performed using scitools (github.com/adeylab/scitools). Additional code used to analyze the data will be made available as a Github repository (github.com/adeylab/sciMAP-ATAC). Raw and processed single cell library sequencing data will be submitted to NCBI Gene Expression Omnibus (GEO; http://www.ncbi.nlm.nih.gov/geo/). All single-cell epigenomics data will be made available through the BRAIN Initiative Cell Data Center (BCDC).

Methods

Sample preparation

All animal studies were approved by the Oregon Health and Science University Institutional Animal Care and Use Committee. Male C57Bl/6J mice aged 8 weeks were purchased from Jackson Laboratories. Animals were sacrificed by carbon dioxide primary euthanasia and cervical dislocation secondary euthanasia. Animals were immediately decapitated, intact brain tissue was harvested, washed in ice-cold phosphate-buffered saline (pH 7.4), submerged in OCT (Cat. TFM-C) within a disposable embedding mold (Cat. EMS 70183), and flash-frozen in an isopentane/liquid nitrogen double-bath by lowering into the isopentane bath without submerging the sample. Samples were immediately transferred to dry ice, paraffin wrapped in order to delay sample dehydration, and stored at -80 °C.

Sample sectioning

Intact embedded whole mouse brains from three mice were sectioned in a cryostat (Leica) at -11°C chuck and chamber temperature and collected on Superfrost Plus microscope slides (Fisherbrand, Cat. 22-037-246). Whole brain sectioning was performed in sets of: one section at 100 µm paired with three sections at 20 µm, in order to generate approximately twenty-five sets of four slides consisting of coronal micro-biopsy (1) and histology (3) sections at one section per slide for each entire mouse brain. Slide boxes were sealed with paraffin in order to prevent sample dehydration and stored long-term at -80°C.

Coronal section mapping and immunohistochemistry

In order to determine the mouse brain atlas coordinate of each coronal microbiopsy section, the histological section immediately adjacent to each microbiopsy section were fixed in 4% PFA for 10 minutes and pan-neuronal stained using 300 µM DAPI (Thermo Fisher, Cat. D1306) in 1x (pH 7.4) PBS (Thermo Fisher, Cat. 10010023) for 5 minutes. Slides were rinsed with 1x PBS and mounted in Fluoromount-G (Thermo Fisher, Cat. 00-4958-02). Slides stained for Satb2 were equilibrated to room temperature and circumscribed with a hydrophobic barrier pen (Invignome, Cat. GPF-VPSA-V). Sections were washed twice with PBS for 10 minutes then blocked for 1 hour at room temperature in permeabilization/blocking buffer comprised of PBS with 10% normal goat serum (Jackson ImmunoResearch, Cat. 005-000-121), 1% bovine serum albumin (BSA, Millipore, Cat. 126626), 0.3% Triton X-100 (TX-100, Sigma, Cat. 11332481001), 0.05% Tween-20 (Sigma, Cat. P1379), 0.3 M glycine (Sigma, Cat. G7126) and 0.01% sodium azide (Sigma, Cat. S2002) for 1 hour at room temperature. During the blocking step, the primary antibody rabbit anti-Satb2 (Abcam Cat. ab92446) was diluted 1:1000 in a buffer containing PBS, 2% NGS, 1% BSA, 0.01% TX-100, 0.05% Tween-20, and 0.01% sodium azide. The diluted primary antibody was applied to sections then incubated overnight at 4°C. The primary antibody was washed from the sections five times with PBS for 5 minutes at room temperature. Secondary antibody AF488 goat anti-rabbit (Thermo Fisher Cat. A32731) was prepared by diluting 1:1000 in the same buffer used to dilute primary antibodies. Sections were incubated with the diluted secondary antibody for 1 hour in the dark at room temperature. Secondary antibodies were washed from the sections three times with PBS for 5 minutes, then nuclei were counterstained with DAPI for 10 minutes at room temperature. After DAPI staining, sections were washed an additional two times then glass coverslips were mounted with ProLong Diamond Anti-Fade Mounting Medium (Thermo Fisher, Cat. P36961). Slides were imaged on a Zeiss ApoTome AxioImager M2 fluorescent upright microscope and processed using Fiji software. Coronal section images were mapped to the Adult Mouse Allen Brain Atlas[22] according to anatomical regions.

Tissue microbiopsy acquisition and nuclear isolation

Tissue microbiopsies were acquired for the somatosensory cortex sciMAP-ATAC (96 MBP) and MBP-derived sci-ATAC-seq preparation from coronal sections throughout the mouse brain (384 MBP). Microbiopsy slides at 200 µm were acclimated to -20C in the cryostat (Leica) and microbiopsy punch tools (EMS, Cat. 57401) were cooled on dry ice prior in order to prevent warming of tissue upon microbiopsy punching. Microbiopsy punches were acquired according to location identified from section mapping, and frozen microbiopsies were deposited directly into 100 µL of ice-cold Nuclear Isolation Buffer (NIB; 10mM Tris HCl, pH 7.5 [Fisher, Cat. T1503 and Fisher, Cat. A144], 10mM NaCl [Fisher, Cat. M-11624], 3mM MgCl2 [Sigma, Cat. M8226], 0.1% IGEPAL [v/v; Sigma, I8896], 0.1% Tween-20 [v/v, Sigma, Cat. P7949] and 1x protease inhibitor [Roche, Cat. 11873580001])) in a 96-well plate. Punch deposition into each well of the 96-well plate was visually confirmed under a dissecting microscope. In order to facilitate tissue dissociation and nuclear isolation, 96-well plates of

microbiopsy punches were then gently shaken (80 rpm) for 1 hour on ice. Mechanical dissociation was then performed via multi-channel pipette at 30 triturations per well. Sample plates were then centrifuged at 500 rcf for 10 minutes. While nuclear pellets were not visible, we found that aspiration of 90 µL of supernatant and resuspension in an added 30 µL of NIB results in a final isolated nuclear volume of 40 µL with approximately 15,000 nuclei per well (for microbiopsy punching conditions: 200 µm section, 250 µm diameter microbiopsy punch). For the somatosensory cortex preparation, nuclei were split across four 96-well plates such that nuclei were aliqotted to 10 µL, or approximately 3,750 nuclei per well. This enabled 4 independent indexed transposase complexes to be utilized for each individual MBP, or 384 uniquely indexed transposition reactions in one experiment.

Whole brain dissociation and nuclei isolation

In order to evaluate the effect of flash-freezing on chromatin accessibility in mouse brain tissue, we evaluated single cell chromatin accessibility profiles from an intact mouse brain in which one hemisphere was flash-frozen as described previously, and one hemisphere remained unfrozen. Both hemispheres were processed separately and underwent dissociation and nuclear isolation. Tissue was diced in Nuclear Isolation Buffer (NIB: 500 µL 10 mM Tris-HCl pH .5, 100 µL 10 mM NaCl, 150 µL MgCl2, 500 µL 0.1% Igepal, 0.1% Tween 20, 1-unit Qiagen Protease Inhibitor, nuclease-free water to 50 mL) in a petri dish on ice using a chilled razor blade. Diced tissue was transferred to 2 mL chilled NIB in a 7 mL dounce-homogenizer on ice. The tissue was incubated on ice for 5-minutes then homogenized via 10 gentle strokes of the loose pestle on ice, a 5-minute incubation on ice, then 10 gentle strokes of the tight pestle on ice. The homogenate was then strained through a 35 µm strainer and centrifuged at 500 rcf for 10 minutes. Samples were then aspirated, resuspended in 5 mL of ice-cold NIB and nuclei were counted on a hemocytometer. Samples were diluted to 500 nuclei per 1 µL in order to facilitate tagmentation reaction assembly at 5,000 nuclei per 10 µL of NIB.

Location indexing via tagmentation

Transposase catalyzed excision of the chromatin accessible regions via tagmentation results in addition of unique molecular identifiers, indexes, for each tagmentation reaction. In order to encode microbiopsy punch location into library molecules, we recorded the corresponding tagmentation well within each 96-well plate to the user-identified microbiopsy punch location. This incorporation of location information required no protocol adjustments to the established sci-ATAC-seq methodology. Tagmentation reactions were assembled at 10 µL of isolated nuclei at 500 nuclei per 1 µL, 10 µL 2x tagmentation buffer (Illumina, Cat. FC-121-1031), and 1 µL of 8 µM loaded indexed transposase was added per well (See Picelli et al. for loading protocol) [27]. Each assembled 96-well plate of tagmentation reactions was incubated at 55°C for 15 minutes. For the whole brain sci-ATAC-seq preparation on fresh and frozen tissue experiment, four 96-well plates of tagmentation were used (384 uniquely indexed tagmentation reactions). For the initial MBP-derived sci-ATAC-seq preparation from whole brain derived punches, four 96-well plates of tagmentation were used (384 uniquely indexed tagmentation reactions). Finally, for the somatosensory cortex sciMAP-ATAC experiment four 96-well plates of tagmentation were used (384 uniquely indexed tagmentation reactions). For whole brain sci-ATAC-seq preparation on fresh and frozen tissue experiment, tagmentation wells were pooled separately for fresh and frozen hemisphere samples. For the MBP-derived experiments, all tagmentation reactions were pooled.

Combinatorial indexing via PCR

In order to terminate transposition, PCR plates are prepared with protease buffer, primers, and sparsely sorted nuclei and then incubated. Post-denaturation, the remaining PCR reagents are added and incorporation of the PCR primers results in incorporation of the secondary index for single combinatorial indexing. For the denaturation step, 96-well PCR plates of 8.5 µL protease buffer (PB; 30 mM Tris HCl, pH 7.5 [Fisher, Cat. T1503 and Fisher, Cat. A144], 2 mM EDTA [Ambion, Cat. AM9261, 20 mM KCl [Fisher, Cat. P217 and Fisher, Cat. A144], 0.2% Triton X-100 [v/v, Sigma, Cat. 9002-93-1], 500 ug/mL serine protease [Fisher, Cat. NC9221823], 1 µL 10 mM indexed i5, and 1uL indexed i7 per well were prepared. Pooled tagmented nuclei were stained by addition of 3 µL of DAPI (5mg/mL) per 1 mL of sample. Each sample was then FAC sorted using a Sony SH800 FACS machine at 88 nuclei per well into prepared 96-well plate(s). Gating was performed to isolate a singlet DAPI stained nuclei. Four PCR plates (384 uniquely indexed wells) were utilized for the initial MBP-derived sci-ATAC-seq preparation from whole brain derived punches, two PCR plates (196 uniquely indexed wells) were used for the somatosensory cortex sciMAP-ATAC experiment, and two PCR plates (196 uniquely indexed wells) were utilized for the whole brain sci-ATAC-seq preparation on fresh and frozen tissue experiment. Transposase denaturation was then performed by sealing each sorted plate and incubating at 55°C for 15 minutes. Plates were immediately transferred to ice

post-incubation and 12 µL of PCR mix (7.5 µL NPM, 4 µL nuclease-free water, 0.5 µL 100× SYBR Green) was added to each well. For each experiment, plates were then sealed and PCR amplified on a BioRad CFX real time cycler using the following protocol: 72°C for 5:00, 98°C for 0:30, Cycles of [98°C for 0:10, 63°C for 0:30, 72°C for 1:00, plate read, 72°C for 0:10] for 18-22 cycles. PCR plates were transferred to 4°C once all wells reached mid-exponential amplification on average. Each PCR plate is then pooled at 10 µL per well and DNA libraries are isolated using a QIAquick PCR Purification column. Each pooled PCR plate library is then quantified using a Qubit fluorimeter, diluted to 4 ng/µL with dH_2O, and quantification of library size is performed on Agilent Bioanalyzer using a high sensitivity chip. Libraries are then sequenced on a NextSeq™ 500 sequencer loaded with custom primers and chemistry, as previously described[16].

Sequence data processing

Data analysis and plotting was performed primarily using the 'scitools' software (github.com/adeylab/scitools)[19], which includes wrappers for a number of external tools. Raw sequence reads had their index combinations matched to a whitelist of expected indexed using 'scitools fastq-dump' which allows for a hamming distance of two and produces error-corrected fastq files. These were then aligned to mouse reference genome (mm10) and sorted using 'scitools align'. PCR duplicate removal and filtering for quality 10 aligned autosomal and chromosome X reads (*i.e.* excluding mitochondrial, chromosome Y, and unanchored contigs) was performed using 'scitools rmdup' using default parameters and plotted using 'scitools plot-complexity'. Projections of passing reads given increased sequencing depth was performed using 'scitools bam-project' on the pre-duplicate removed bam file, which generates a model for each single cell based on sampling reads and calculating the passing read percentage which we find to be within 2% accuracy[16]. Bam files were then filtered to only contain cell barcodes that were ascribed to true single cells based on the complexity files produced by 'scitools rmdup' by running 'scitools filter-bam' with -n corresponding to the read threshold for true cells. This filtered bam was then used for assessing transposase plate performance using 'scitools index-performance'. Cell renaming was performed using 'scitools rename-cells'.

Chromatin accessibility analysis

The filtered bam file was used for chromatin accessibility peak calling for each of the preparations individually as well as on a combined bam file of all preparations. Peak calling was run using the wrapper function 'scitools callpeak' which utilized macs2 for peak calling and then filtering and peak extension to 500bp. Called peaks from all datasets were merged to generate a union peak set that was used for all subsequent analysis. The peak bed file and filtered bam file were then used to construct a counts matrix of cells × peaks. Latent Dirichlet Allocation using the package cisTopic[28] was performed using the scitools wrapper function 'scitools cistopic'. The cells × topics matrix was biclustered and plotted using 'scitools matrix-bicluster' which utilizes the complexHeatmap library in R. Two-dimensional visualization was performed using UMAP via 'scitools umap' and plotted using 'scitools plot-dims'. Visualization of topic weights on the UMAP coordinates was performed using 'scitools plot-dims' with -M as the cells × topics matrix. Clustering was performed on the cells × topics matrix using the R package phenoGraph which employs Louvain clustering and was executed using the wrapper function 'scitools matrix-pg'. In addition to topic analyses, we utilized ChromVAR[29] to assess the global motif accessibility profiles of cells using the wrapper function 'scitools chromvar' on the bam file with added read group tags using 'scitools addrg'.

Cell type identification

The identified clusters were assigned to their respective cell type by examining the chromatin accessibility profile of marker genes that correspond to known cell types. Gene regions were plotted using 'scitools plot-reads' using the filtered bam file. Additional support for identified cell types was performed by assessing the chromVAR results for global motif accessibility. Marker genes used for cell type identification included: *Gfap*, *Glul,* and *Agt* for astrocytes, *Ppdn* for ependymal cells found to be present within a primarily astrocyte cluster, *Col19a1* for all neuronal cell types, *Gad1, Gad2, Pvalb, Dlx1* and *Dlx2* for GABAergic neurons, *Drd1a, Drd2, Bcl11b* and *Ppp1r1b* for GABAergic medium spiny neurons (MSNs), also referred to as spiny projection neurons (SPNs), *C1qa, C1qc, Cx3cr1* for microglia, *Mrc1* for macrophages within the microglia cluster, *Kdr* and *Flt1* for endothelia, *Olig1* for al oligodendrocyte cell types, *Top2a* and *Cspg4 (NG2)* for OPCs, *Fyn* and *Prox1* for newly formed oligodendrocytes, and *Mobp, Mog, Cldn11* and *Prox1* for mature myelinating oligodendrocytes.

Pseudospatial single-cell ordering

The layer specific characteristics of excitatory neurons (EN) of the cortex provided a previously described, well-annotated, spatially resolved biological system from which to validate sciMAP-ATAC. ENs specifically demonstrate layer specific

characteristics, therefore, cell type identified excitatory neurons derived from our somatosensory cortex (SSC) sciMAP-ATAC experiment dataset (n=2,458), whole brain sci-ATAC-seq preparation on fresh and frozen tissue (n=519), our initial MBP-derived sci-ATAC-seq preparation from 384 whole brain derived punches (n=1,305). The isolates EN read bam file was re-submitted to chromatin accessibility analysis (described above) in order to generate an EN specific counts matrix, called peak bed file, cisTopic matrix, and UMAP dimensions. The union set of EN cells were clustered using Louvain phenoGraph clustering (described above) using -k 500. Five clusters were identified, one of which contained only whole brain derived cells and was excluded due to insufficient spatial information since no spatially resolved cells co-clustered. In order to determine the locations of cortical "Outer" and "Inner" punches within the UMAP projection of the 4,282 ENs, cells were colored by punch orientation using 'scitools plot-dims'. Polarity of the EN UMAP cluster by "Outer" and "Inner" punches allowed us to orient the progression of ENs within the SSC from "Outer" cortex, or approximately layers 2-4, to "Inner" cortex, or approximately layers 4-6". We note that layer 1 is excluded due high dendrite and axon collaterals and a dearth of neuronal cell bodies[30]. To order cells from L2-6 within the UMAP projection of chromatin accessibility, a principal curve was projected through the EN UMAP dimensions. Cells are then projected onto the principle curve and assigned lambda values corresponding to ordering, which we termed "pseudospace". Principal curves were projected through SSC sciMAP-ATAC ENs, and ENs from the union dataset ENs using "scitools dims-pcurve" with -M to subset cell by experiment. UMAP projections illustrating pseudospace were generated using "scitools plot-dims" with -V for principal curve lambda file for the SSC EN-only projection (lambda=0.000-6.737) and union EN projection (lambda=0.000-15.867) where increasing lambda corresponds to progression from inner to outer cortex.

Marker gene normalized read count analysis

In order to assess chromatin accessibility at layer specific genes, normalized read count per cell was calculated for cells ordered by pseudospace according to lambda value, for aggregate EN groups in order to compare "Outer" vs. "Inner" normalized read count for SSC sciMAP-ATAC ENs, and EN sub-clusters (n=4) normalized read count for union dataset ENs. Read count for a given gene for each cell was calculated using "scitools plot-dims" for the mm10 mouse reference genome for a given marker gene, with -X to retain intermediate data files. Intermediate files ".data" and ".gene_data" were then merged in R and subset to EN cell reads between the given gene start and end sites for each cell. Normalized read count was then calculated by dividing the total number of reads with a given gene by the total number of reads within a given cell, in order to eliminate cell read depth bias. The mean normalized read depth per cell was then calculated across EN groups: "Outer"-derived ENs and "Inner"-derived ENs for SSC ENs, and for each of the four EN sub-clusters from the union dataset. Barplots of mean normalized reads per cell were generated using *ggplot geom_barplot* plotting function (v3.1.0).

Transcription factor enrichment along pseudospace

ChromVAR analysis was rerun on the union dataset ENs as described above. The ChromVAR transcription factor motif accessibility output was Z-scored and subset to the list of transcription factors detailed previously [26]. A smoothed curve was fit to each transcription factor across pseudospace-ordered ENs. Smoothing was performed with by a LOESS model with R functions loess and predict with a given interval of 100 equal subdivisions of the pseudospace range. Predicted curves values were cast into a pseudospace × transcription factor matrix and transcription factors were ordered by their maximum value in pseudospace. The resulting matrix was plotted via ComplexHeatmap (v1.2.0.0; Fig. 3g). To ensure data was not over-smoothed, the same ChromVAR output was used to generate a heatmap based on average Z-scored motif accessibility categorized by the EN sub-clusters (as in Fig. 3d) with similar results (Extended Data Figure 5).
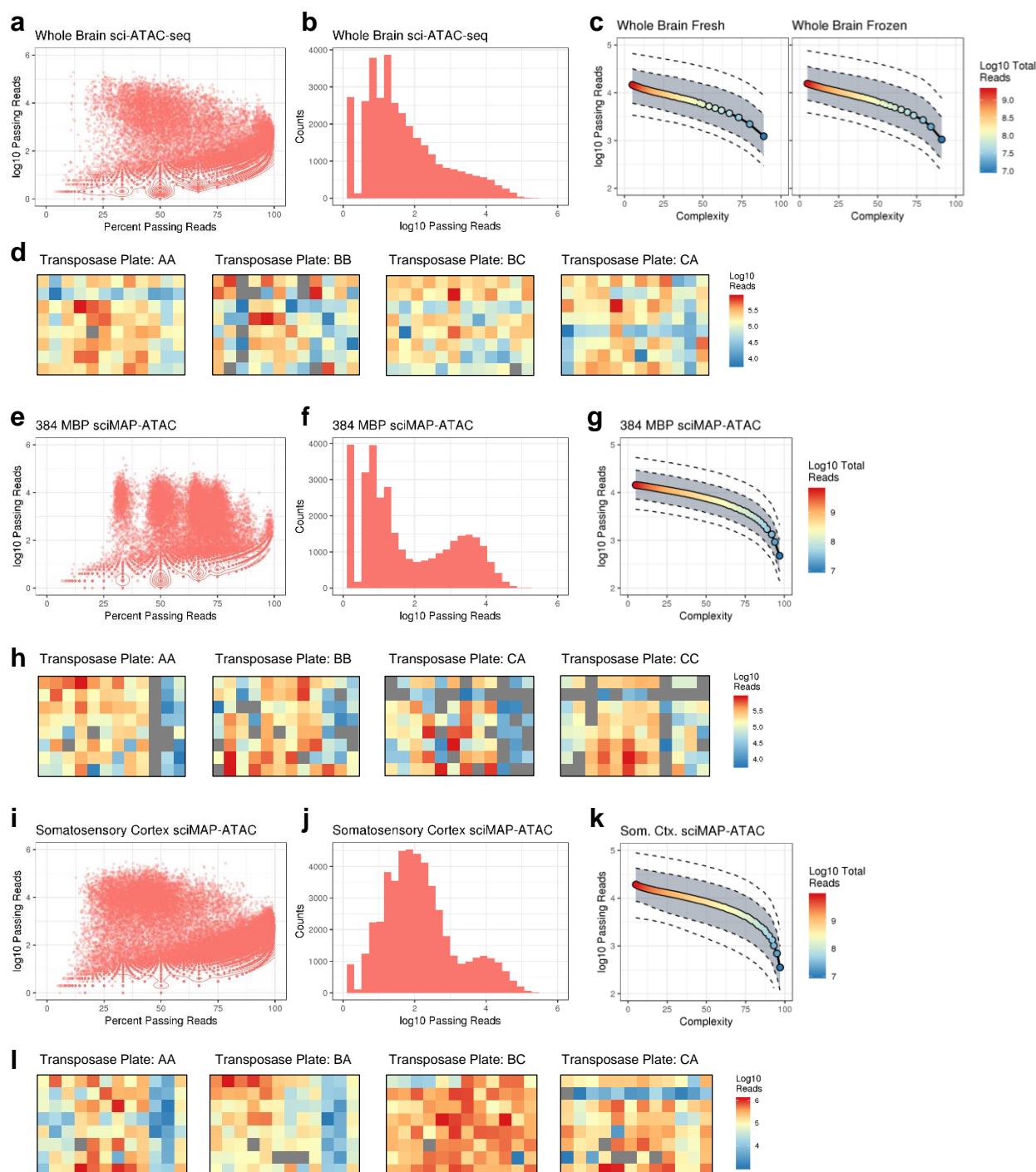
Extended Data Figure 1 | Library Quality Assessment. a. Library complexity for the standard sci-ATAC-seq workflow on fresh and frozen mouse brain tissue. Log10 total passing reads per index combination are plotted with respect to the percentage of passing reads (Methods). **b.** Histogram of the log10 passing reads per index combination shows the typical bimodal separation of cells and debris. **c.** Projected passing reads per cell split by fresh or frozen tissue samples. Solid line with points is the median passing reads per cell with respect to the log10 raw reads sequenced (color), ribbon indicates the 25th to 75th percentile of cell projections, and the outer dashed lines indicate the 10th and 90th percentiles of projections. **d.** Log10 passing reads from passing cells based on the transposition well. **e-h.** As in **a-d**, but for the 384 microbiopsy punch sci-MAP-ATAC test preparation. **i-l.** As in **a-d**, but for the sciMAP-ATAC preparation on the mouse somatosensory cortex.
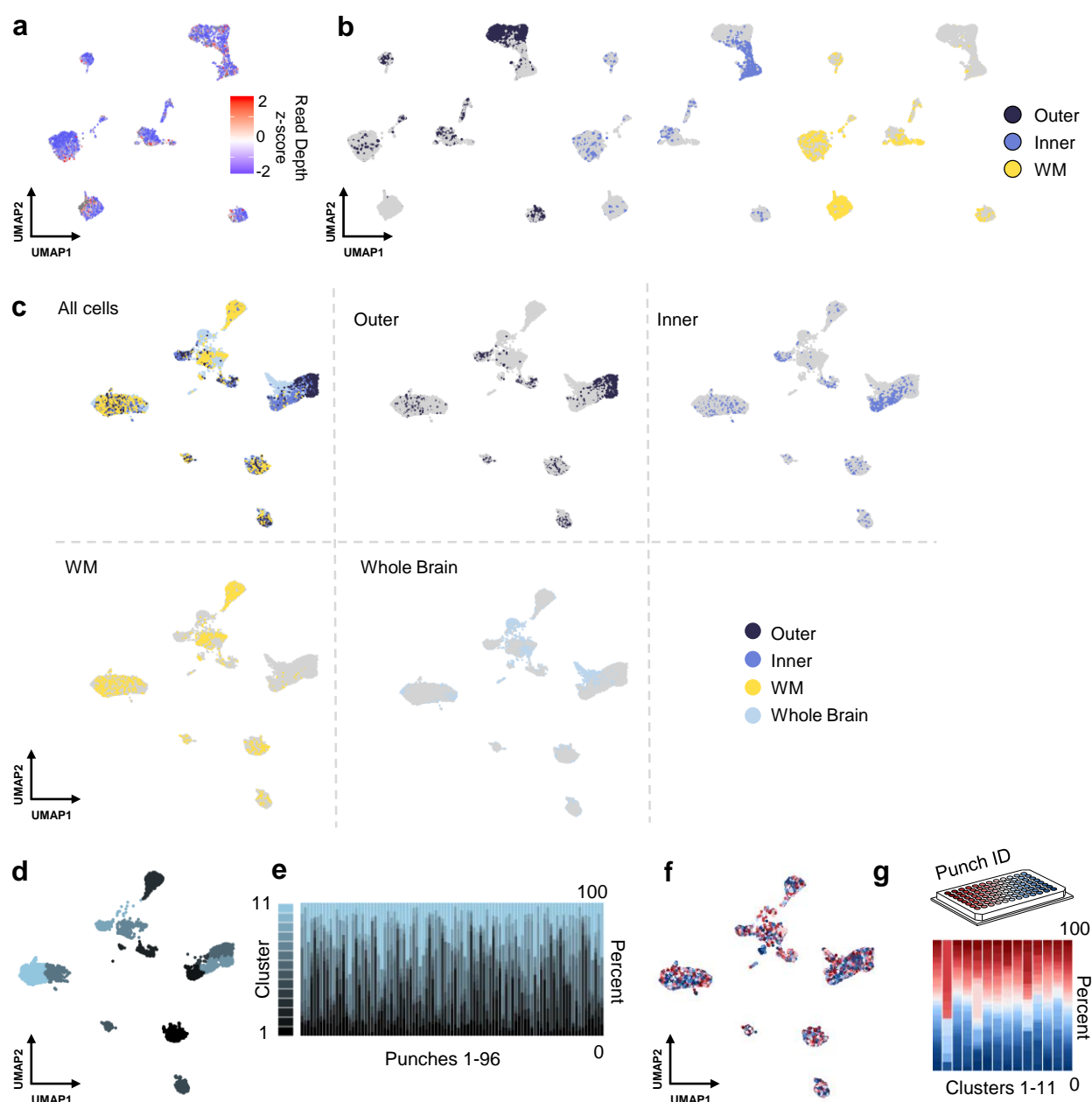
Extended Data Figure 2 | Quality metrics and microbiopsy punch compositions from sciMAP-ATAC. a. sciMAP-ATAC cells from the somatosensory cortex projected into two-dimensions and colored by the read depth z-score. **b.** Two-dimensional representation of cells from the combined dataset including non-spatial, 384 microbiopsy, and somatosensory cortex preparations. Only cells from the somatosensory cortex are shown and are colored by the clusters that were identified. **c.** Cluster identity proportions for each of the 96 microbiopsy punches in the somatosensory cortex sciMAP-ATAC preparation. **d.** Cells are represented as in **b**, but colored by individual microbiopsy punch. **e.** Percentage of each microbiopsy punch in each cluster (as shown in **b**).
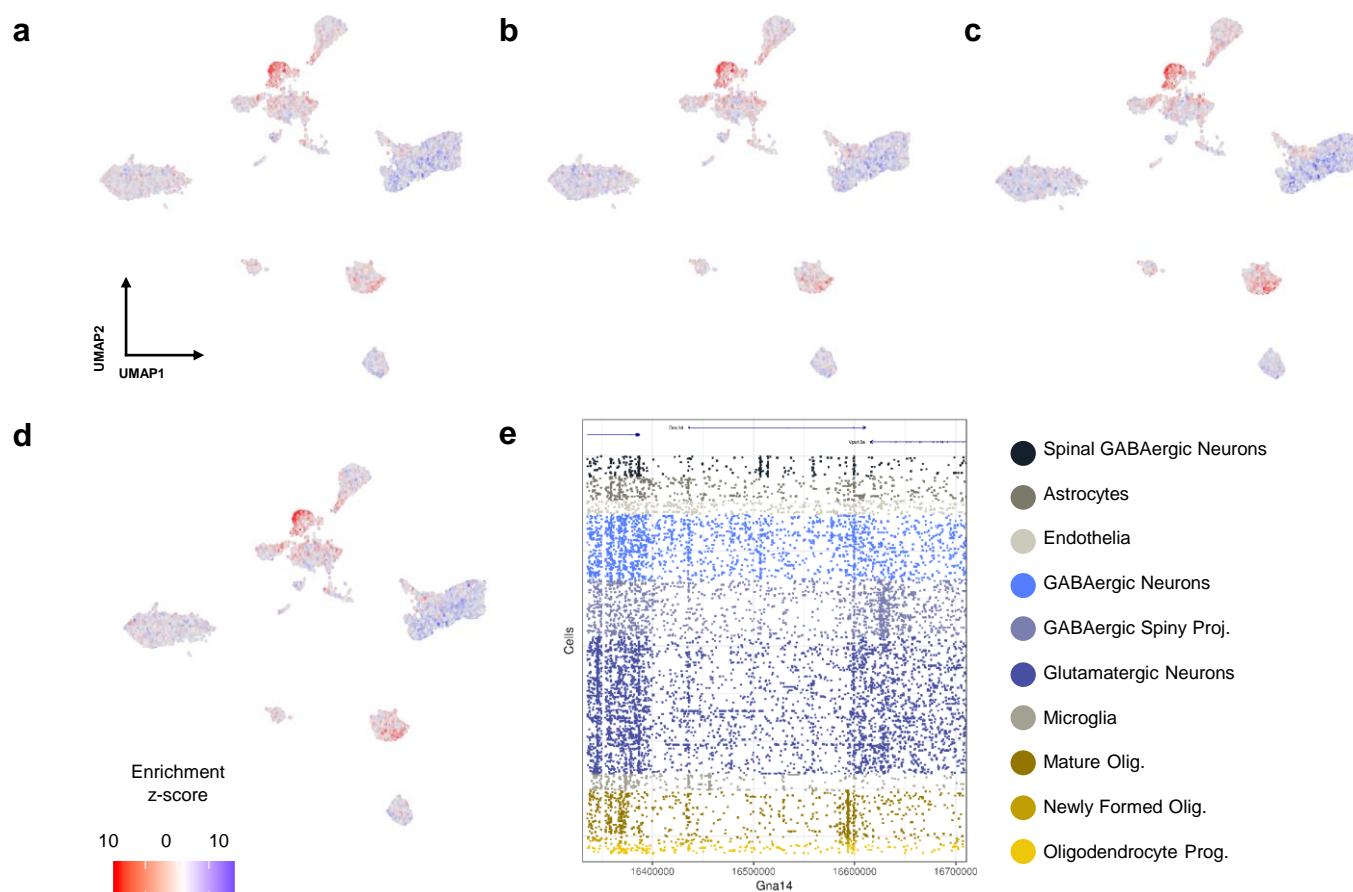
Extended Data Figure 3 | Whole brain-only cluster identified as spinal cord derived interneurons. TF motif enrichment for spinal column identifier TFs across all cells in union dataset for **a.** HOXA **b.** HOXB **c.** HOXC and **d.** HOXD **e.** Chromatin accessibility signal at spinal cord marker gene Gna14. Each row is the signal for a single cell across the genomic region, colored by cell type annotation.
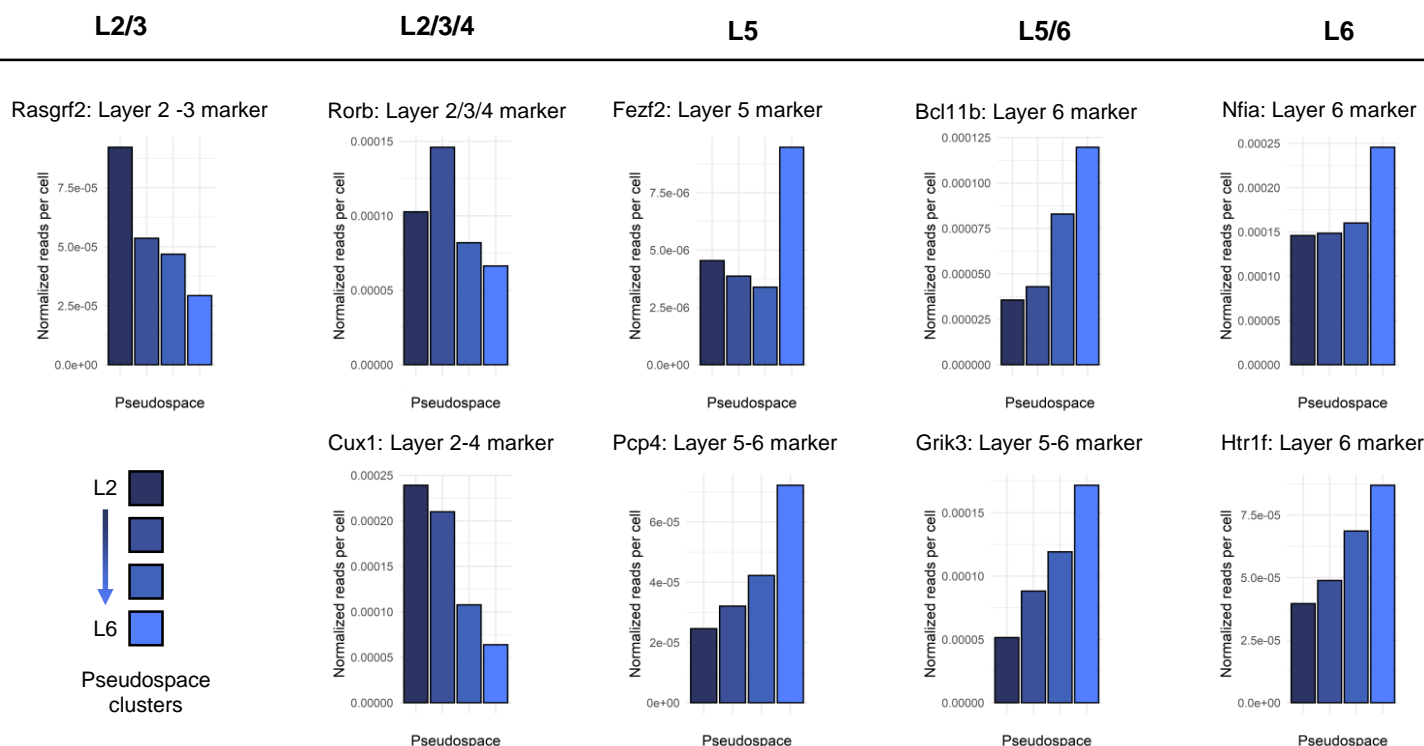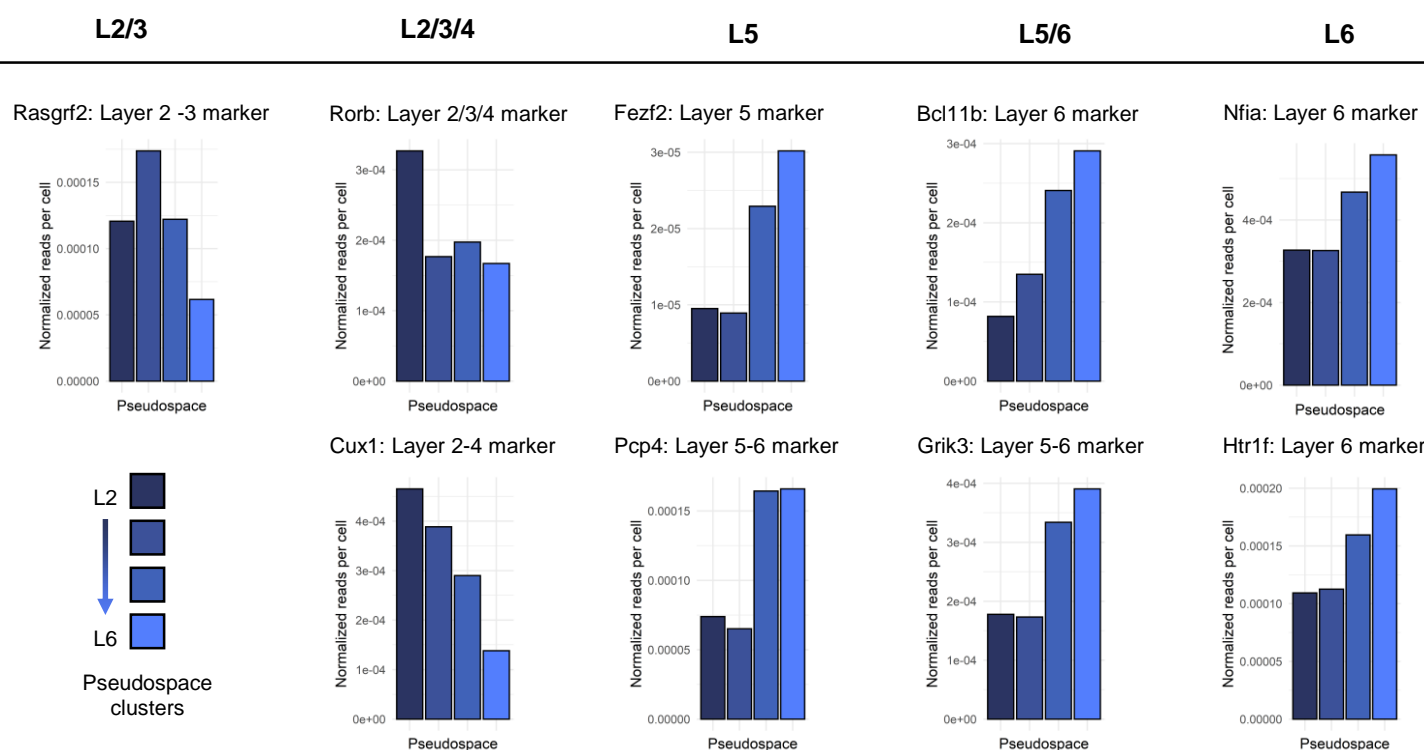
Extended Data Figure 4 | Cortical layer marker chromatin accessibility across pseudospace. Layer-specific marker gene accessibility measured by normalized reads per cell for four pseudospace ordered excitatory neuron sub-clusters. **a.** Marker gene accessibility in sciMAP-ATAC somatosensory cortex excitatory neurons only. **b.** Marker gene accessibility for union dataset excitatory neurons.
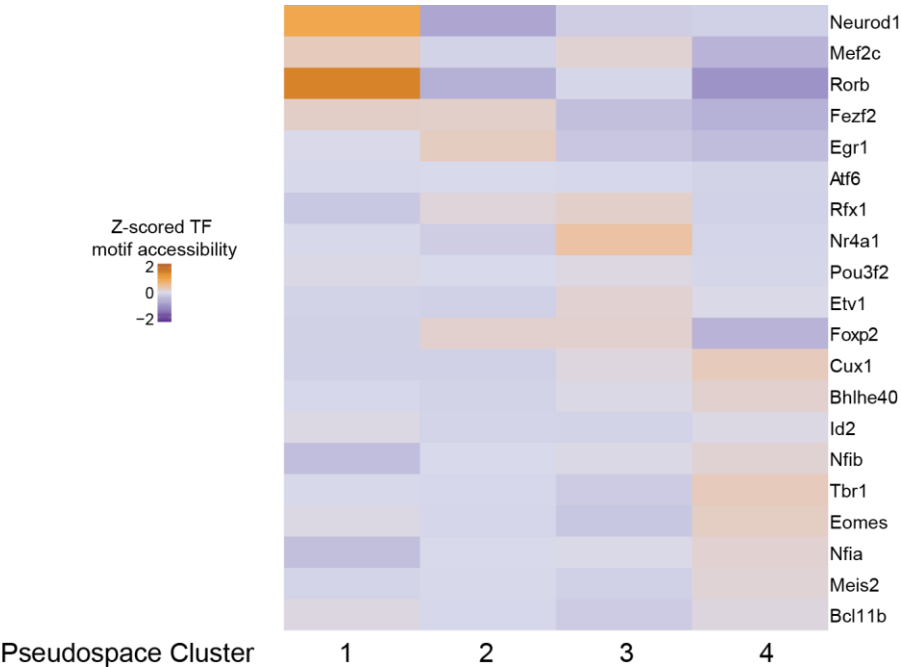
Extended Data Figure 5 | Average ChromVAR Z-Scored transcription factor accessibility for union Ens aggregated by pseudospace cluster. Union EN clusters through pseudospace are consistent with Figure 3g and reflect chromatin differences between cortical layers.